

Ensemble Patterns of Hippocampal CA3-CA1 Neurons during Sharp Wave–Associated Population Events

Jozsef Csicsvari, Hajime Hirase,
Akira Mamiya, and György Buzsáki*
Center for Molecular and Behavioral
Neuroscience
Rutgers University
The State University of New Jersey
Newark, New Jersey 07102

Summary

Transfer of neuronal patterns from the CA3 to CA1 region was studied by simultaneous recording of neuronal ensembles in the behaving rat. A nonlinear interaction among pyramidal neurons was observed during sharp wave (SPW)–related population bursts, with stronger synchrony associated with more widespread spatial coherence. SPW bursts emerged in the CA3a–b subregions and spread to CA3c before invading the CA1 area. Synchronous discharge of >10% of the CA3 within a 100 ms window was required to exert a detectable influence on CA1 pyramidal cells. Activity of some CA3 pyramidal neurons differentially predicted the ripple-related discharge of circumscribed groups of CA1 pyramidal cells. We suggest that, in SPW behavioral state, the coherent discharge of a small group of CA3 cells is the primary cause of spiking activity in CA1 pyramidal neurons.

Introduction

The CA3 region, with its extensive recurrent collateral system (Ishizuka et al., 1990; Li et al., 1994), is thought to be a critical site for hippocampal function (Marr, 1971; McNaughton and Morris, 1987; Buzsáki, 1989; Wilson and McNaughton, 1994; Muller et al., 1996; Skaggs et al., 1996; Lisman, 1999; Rolls, 1999). Despite its postulated prominent role in computation, few studies have examined the specifics of CA3 neuronal activity in behaving animals. In most studies, units recorded from CA1 to CA3 fields are reported to have grossly similar behavioral correlates and are analyzed together as a single group (McNaughton et al., 1983; Muller et al., 1987; O'Keefe and Recce, 1993; Deadwyler et al., 1996; Tanila et al., 1997; Wiebe and Staubli, 1999). Thus, it is not clear what kind of specific computation is added by the CA1 region to the information already available at the CA3 output.

Understanding the processing of representations by brain structures requires precise information about the nature of the input. For example, unique spatiotemporal discharges of neurons in the mushroom bodies in the locust have been found to characterize the various features of olfactory stimuli (Laurent, 1999). In cortical association areas such as the hippocampus, the detailed structure of the input is not known. Furthermore, in the

multisynaptic hippocampal circuits (Amaral and Witter, 1989), processing of information occurs during macroscopic oscillations (Buzsáki and Chrobak, 1995). Studying the contribution of the individual hippocampal regions to the overall performance is difficult during oscillatory states because oscillations tend to synchronize all neurons in the circuit.

In the immobile and sleeping rat, irregularly occurring sharp waves are observed in the CA1 stratum radiatum (Buzsáki et al., 1983). During these behavioral states, the release of subcortical neuromodulators is substantially reduced, and, as a consequence, the spread of activity in the CA3 collateral system is disinhibited (Hasselmo et al., 1995). During SPWs, neurons in layers II–III of the entorhinal cortex, the main cortical inputs to the hippocampus, are relatively silent (Chrobak and Buzsáki, 1994). Furthermore, lesions of the entorhinal cortex facilitate the incidence of hippocampal SPW-associated population bursts (Bragin et al., 1995). Thus, hippocampal SPWs are believed to represent an intrinsic network pattern of the hippocampus, present at times when subcortical and cortical influences are reduced. Hippocampal SPW bursts, therefore, allow for the investigation of ensemble bursting in the CA3 region and the nature of signal propagation between the CA3 and CA1 regions.

The emerging population burst in the CA3 region (Traub and Wong, 1982; Buzsáki et al., 1983; Traub and Bibbig, 2000) is believed to give rise to the depolarization of the apical dendrites of CA1 neurons, reflected as a negative SPW in the stratum radiatum. The discharging CA3 and recruited CA1 pyramidal cells also excite CA1 basket and chandelier cells, which, in turn, give rise to a transient fast oscillatory “ripple” (140–200 Hz) in the pyramidal cell layer (Buzsáki et al., 1992; Ylinen et al., 1995). These ripples are reliable indicators of the occurrence of SPWs and are relatively easy to detect. In the present work, using the SPW-associated ripples, we studied the emergent synchrony of pyramidal cell and interneuron ensembles in the subfields of the CA3 and CA1 regions.

Results

Variability of Ripple Power in the CA1 Region

On average, ripples are assumed to be coherent along the long axis of the CA1 region (Chrobak and Buzsáki, 1996). However, when individual oscillatory episodes were considered, a considerable location-dependent variability became evident (Figure 1A). To quantify these observations, the simultaneously recorded fields from the CA1 region with arrays of electrodes (Figure 1A, inset) were digitally filtered (80–250 Hz) and the power (root-mean-square) was calculated for the traces derived from each electrode. The peak of the resulting envelope was used as a reference event for calculating time correlations (Csicsvari et al., 1999a, 1999b). Ripples recorded from each electrode were arbitrarily classified into four amplitude categories on the basis of ripple power. Cross-correlation of the peaks of the envelope

* To whom correspondence should be addressed (e-mail: buzsaki@axon.rutgers.edu).

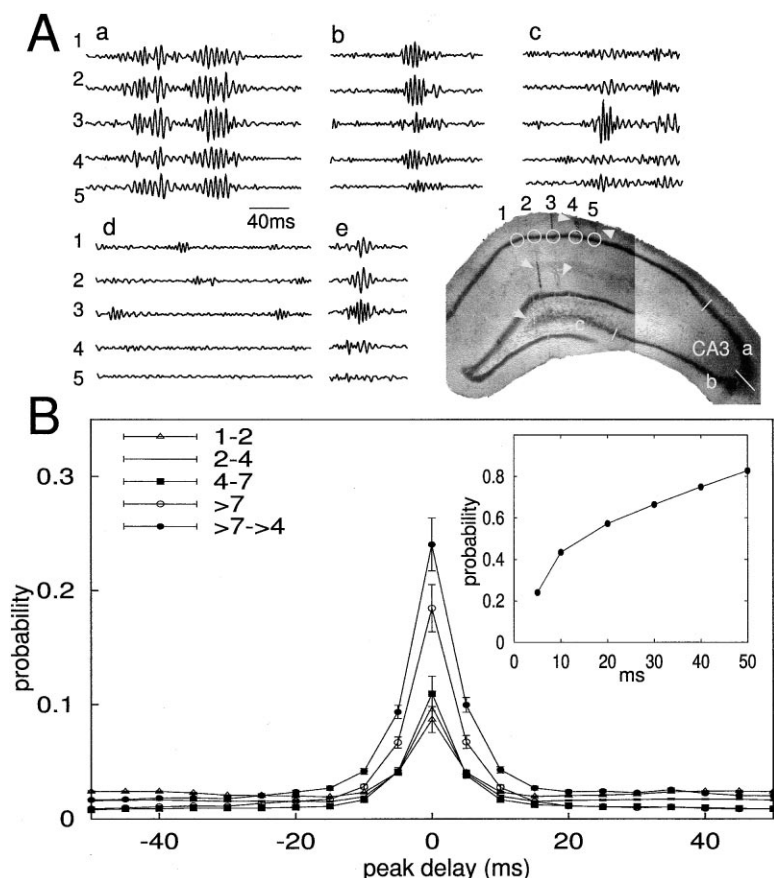


Figure 1. Variability of Local Fast Frequency Oscillations in the CA1 Region

(A) Simultaneously recorded field potentials at five adjacent CA1 sites (filtered: 80–250 Hz). (Inset) Circles, position of the recording sites; arrowheads, tracks of the recording tetrodes 300 μ m apart. Lines indicate the boundaries between CA3 subregions (a, b, and c).

(Aa) Large amplitude ripples (>7 SD from baseline) are present at all recordings sites and show a similar pattern.

(Ab and Ac) Examples of amplitude variability of ripples with similar frequency.

(Ad) Low-amplitude (<4 SD) fast field oscillation confined to one or two recording sites.

(Ae) Frequency variation across electrode sites. Note a fast (>180 Hz) event on electrode 3, simultaneously present with slower (110 Hz) oscillations on electrodes 1 and 2.

(B) Averaged cross-correlograms (mean \pm SE) of peak times of fast field oscillations at different recording sites. The various curves indicate cross-correlograms between events recorded from all combinations of the recording sites. For the calculations of the histograms, the peak of the integrated power (root-mean-square) of the filtered field (80–250 Hz) was used. Symbols correspond to the magnitude of the events (times SD from baseline) that were used for the construction of the correlograms. (Inset) Cumulative probability function of the cross-correlation function for events >7 SD on one site and >4 SD on the other site in a given time window. In a 50 ms window, the probability that the peak of a large amplitude ripple (7 SD) occurred together with oscillatory events (>4 SD) at another site exceeded 0.8.

of integrated field ripples from electrode pairs revealed that spatial coherence (Bullock et al., 1995) depended on the magnitude of the ripple event; coherence of large amplitude ripples was high (Figures 1Aa and 1B), whereas the small amplitude events remained spatially localized (Figures 1Ad and 1B). The probability that the peaks of larger amplitude ripple episodes (>4 SD from baseline) occurred within a 50 ms window exceeded 0.8 (Figure 1B, inset). Although the cross-correlations indicated that, on average, local ripples developed and peaked at the same time, individual events could be “initiated” from any location. Thus, no particular recording site systematically “lead” the ripple event.

Local ripples were correlated with single unit activity derived from the same electrode or from other electrodes (Figure 2A). The local field was always better correlated with the activity of local pyramidal cells than with units recorded from distal sites (≥ 300 μ m). Importantly, this difference was largest for small amplitude ripples and diminished substantially with increasing ripple size (Figure 2B, inset). In contrast, interneurons showed less spatial specificity by having similar correlations with both locally and distally derived fields, independent of the ripple amplitude. In summary, these findings revealed that large amplitude ripple events have a high spatial coherence, whereas small amplitude events tended to remain localized.

CA3-CA1 Projection Topography Affects Spatial Coherence of Ripples

The extent of the intrinsic connectivity of various CA3 subregions (CA3a, b, and c), as well as their projection to the CA1 region, varies (Ishizuka et al., 1990; Li et al., 1994). This anatomical inhomogeneity and theoretical work (Traub and Wong, 1982) indicates the importance of the density of recurrent connectivity in determining the dynamics of population bursts. Therefore, we separately analyzed unit activity recorded from the three CA3 subregions. Similar to the CA1 region, CA3 pyramidal neurons in all subregions increased firing rates during CA1 ripples. Both the ripple-associated firing rate increase (Figure 3A) and the degree of population synchrony (Figure 3C) were more robust in CA1 than in the CA3 region. Within the CA3 population, neurons in the CA3c subregion displayed the largest dynamic range during CA1 ripples, followed by neurons in CA3b and CA3a (Figure 3A). On the other hand, the peak of the CA1 ripple-associated discharge synchrony occurred earlier in CA3a and b ($p < 0.01$, t tests) and progressed to CA3c (Figure 3A, inset). In addition to the peak differences, the rising phases of the amplitude-normalized CA3 histograms shifted earlier (6–20 ms), as reflected by the significantly larger values at -30 ms from the ripple peak ($p < 0.02$ for CA3a, b, and c versus CA1). These observations suggest that population synchrony

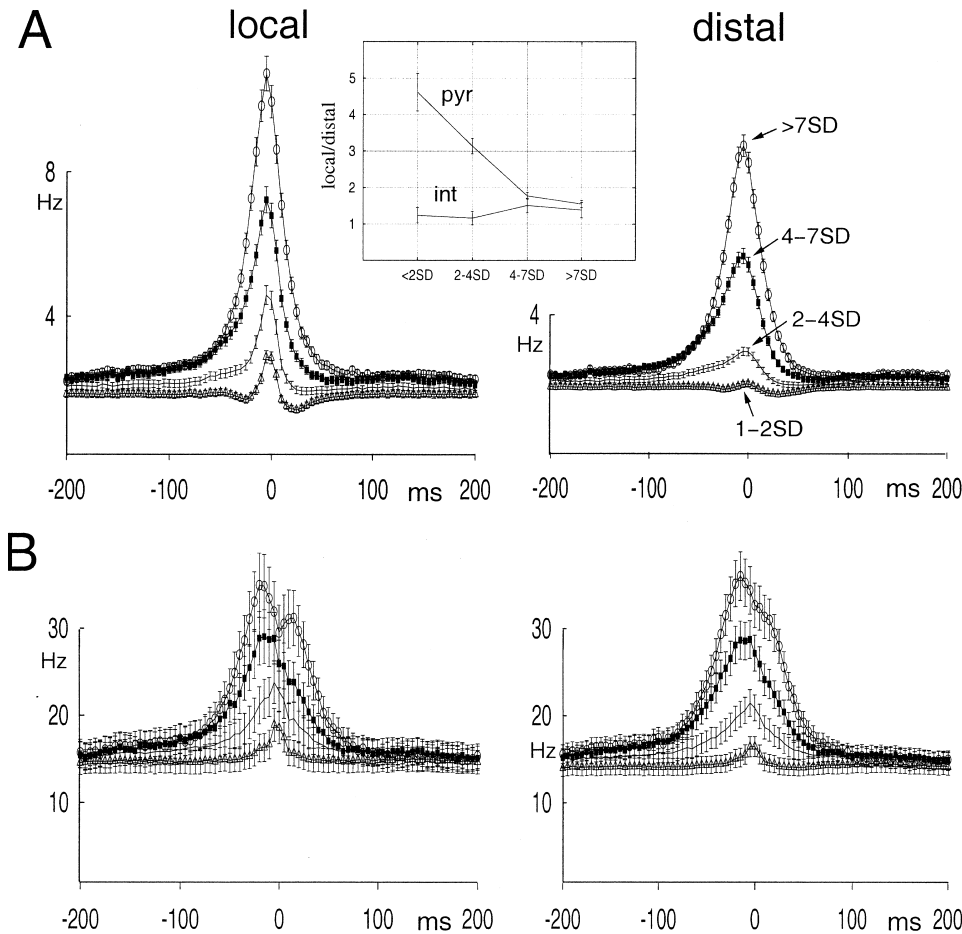


Figure 2. Spatial Coherence of Fast Oscillatory Fields Depends on Ripple Magnitude

Firing rate histograms of CA1 pyramidal cells ([A]; $n = 294$) and interneurons ([B]; $n = 53$) relative to locally detected ripples (local) and ripples detected on a neighboring tetraode (distal; $>300 \mu\text{m}$). Histograms with various magnitude ripples (<2 SD, two to four times SD, four to seven times SD, and >7 SD) are shown separately. (Inset) Ratios of firing rate histogram peaks. Note the difference between unit and local versus neighbor ripple events.

is initiated in the CA3a-b subregions and propagates to CA3c and then to the CA1 region. In contrast to pyramidal cells, ripple-related timing of CA1 and CA3a-b interneurons showed no location-specific differences (Figure 2B). The perievent histograms of individual CA1 interneurons had either a single peak, coinciding with the center of the ripple, or two peaks, before and after the center of the ripple (Csicsvari et al., 1999a). The two peaks in the group histogram in Figure 2B are due to the inclusion of the "double-peak" interneurons. Interneurons in CA3a and b had a single peak. Of the eight recorded CA3c interneurons, six belonged to the SPW-independent group (Csicsvari et al., 1999a). The remaining two interneurons had single peaks associated with the middle of the CA1 ripple.

Discharges of Single CA3 Pyramidal Cells Predict Location-Specific Ripples in CA1

Analysis of the correlations between single CA3 neurons and CA1 field activity indicated further that the location-dependent variability of CA1 ripples can, at least partially, be accounted for by the activity of CA3 neurons.

Figure 4 illustrates the correlation of two CA3 pyramidal neurons with ripples recorded from two CA1 sites. Although the CA1 recording sites had similar amplitude ripples (Figure 4A), only one of the sites showed a correlated discharge with one of the CA3 neurons (Figure 4B). For quantifying the differential involvement of single neuron discharges in CA1 ripple events, differences of the histograms for two CA1 recording sites were calculated (e.g., histogram 1a-3b was subtracted from histogram 1b-3b in Figure 4B). The histograms were considered to be significantly different if the difference between the peak values was larger than three SD of baseline ($p < 0.002$). Of the 543 CA3 pyramidal cell-CA1 recording site combinations, 61 (11%) showed significantly different discharge probability with different CA1 sites (Figure 4C). Although several CA3 pyramidal cells were recorded simultaneously with a tetraode, typically, only one or none of them had a spatial specificity to a given CA1 recording site. Thus, it was not the exact spatial location of the CA3 neurons or the distance between the CA3 and CA1 recording sites that determined whether a given neuron differentially correlated with CA1

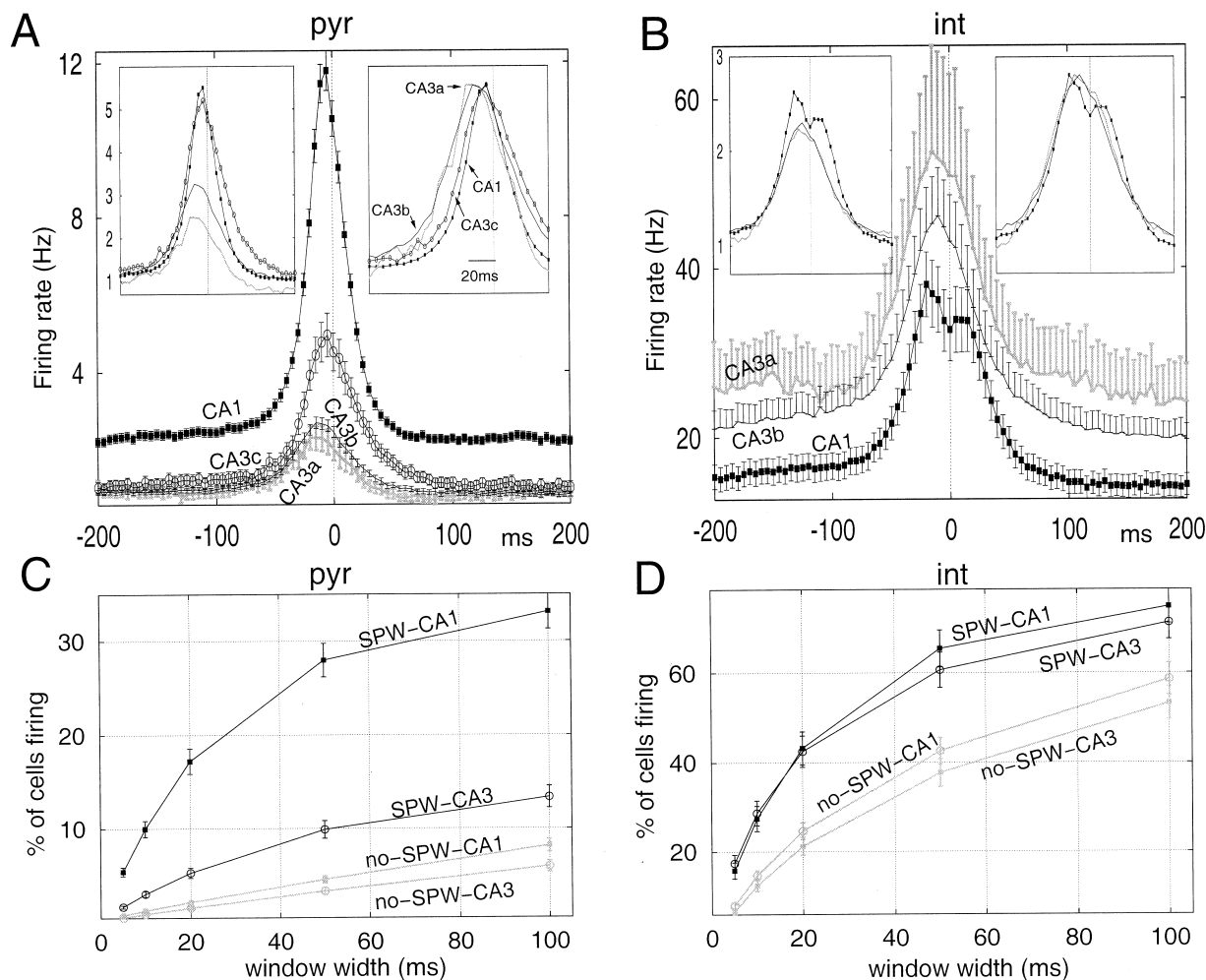


Figure 3. Differential Contribution of CA3 Subregions to CA1 SPW Ripples

Firing rate (A and B) and synchrony (C and D) in CA3 and CA1 neurons during SPW-associated ripples. Firing rate changes (mean \pm SE) of pyramidal cells (A, pyr) and interneurons (B, int) were measured in 5 ms windows, in reference to the peak of SPW-associated ripples (time zero).

(Left inset) Relative changes of cell firing were calculated by dividing firing rate during the ripple by the baseline firing rate, as estimated by the average of bins between -250 to -200 ms.

(Right inset) Amplitude-normalized traces. Note the earlier onset and peak of CA3a ($n = 78$) and CA3b ($n = 287$) pyramidal cell curves relative to CA1 ($n = 294$) and CA3c ($n = 58$) pyramidal cells and the similar time course of CA3a ($n = 9$), CA3b ($n = 52$), and CA1 ($n = 53$) interneurons. (C and D) Average synchrony, determined as the percentage of discharging pyramidal cells (C) and interneurons (D) in 5, 10, 20, 50, and 100 ms time windows. Time windows were centered at the peak of SPWs or consecutively during "no-SPW" epochs. Note large dynamic range of CA1 pyramidal cells relative to CA3 pyramidal neurons but little difference between CA3 and CA1 interneurons.

ripples. Furthermore, location-dependent correlations did not depend on the distance between the CA1 recording sites. Most of the spatial-specific correlations (38 of the 61) were observed between neighboring tetrodes (300 μ m tip separation), commensurate with the larger number of electrode pairs at this distance.

Discharge Rates and Synchrony in CA1 and CA3 Regions

We measured population synchrony (defined as the percent of discharging pyramidal cells in 5–100 ms time windows) separately in the CA3 and CA1 regions (Figures 3C and 3D), during large amplitude ripples (>7 SD) and compared it with "no-SPW" epochs. Enhancement of population synchrony of CA1 pyramidal cells during

ripples was greater than two times larger than that of CA3 pyramidal neurons (Figure 3C). In contrast, ripple-associated population synchrony of interneurons was similar in the CA3 and CA1 regions (Figure 3D).

The number of neurons firing in a given time window (synchrony) can increase, because of an overall increase of firing rates of the individual neurons or by a timing mechanism, without changes in firing rates (Ahissar et al., 1992; Buzsaki et al., 1992). To address this issue, we compared population synchrony and the firing rate changes of the participating neurons (Figure 5A). A sliding time window of 100 ms was used, because this epoch approximated the firing rate changes of neurons during SPW ripples (e.g., Figure 2). Firing rates of neurons were assessed independently of the population

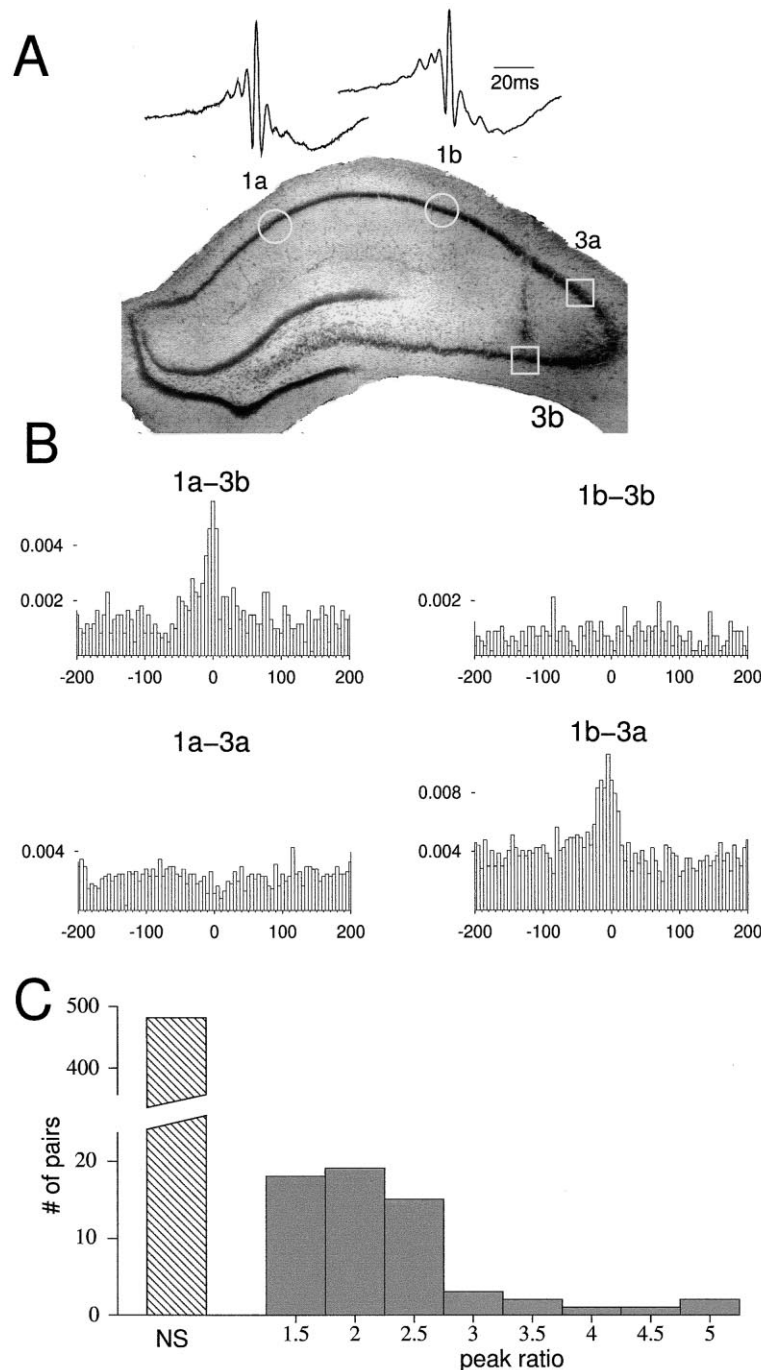


Figure 4. Single CA3 Pyramidal Cells Differentially Predict SPW Ripples at CA1 Recording Sites

(A) Averaged ripples at two CA1 recording sites (1a, 1b on the histological section). Wide-band recordings (1–5 kHz). White squares, recording sites of single CA3 pyramidal cells (3a and 3b). Tracks 1a and 1b were 600 μ m posterior to track 3b.

(B) Cross-correlation of unit firing of the CA3 pyramidal cells with “medium-size” CA1 ripples (four to seven SD) at sites 1a and 1b. Note that CA3 units recorded at sites 3a and 3b selectively correlated with ripples recorded at sites 1b and 1a, respectively.

(C) Histogram of the peak ratios (e.g., histograms 1a-3b/1b-3b in [B]) for all CA3 pyramidal cell-CA1 recording site combinations ($n = 543$). Cross-correlation pairs were considered to be significantly different if the difference between their peak values were larger than three SD of baseline ($p < 0.002$). Baseline SD was measured for bins -250 to -200 ms. NS, number of cell field correlation pairs without significant ratios ($n = 482$).

synchrony (Figure 5A; see also Experimental Procedures). For these measurements, long continuous records (>30 min) obtained during immobility and slow-wave sleep were used, irrespective of the field events. This comparison revealed large differences between the two regions. First, the same degree of population synchrony (e.g., 15%) in CA3 was achieved with significantly lower average firing rates ($1.5 \text{ Hz} \pm 0.07$) than in the CA1 region ($2.5 \text{ Hz} \pm 0.15$). Second, doubling the population synchrony was associated with relatively larger frequency changes of CA3 compared to CA1 pyramidal neurons. Figure 5 also reveals that $<10\%$ synchrony

of the recorded CA3 population does not appreciably change the firing rates of CA1 pyramidal neurons. Both CA3 and CA1 pyramidal cells displayed a nonlinear increase of their firing rate with increases of network synchrony.

Cooccurrence of neuronal discharges within a given time window (i.e., synchrony) can occur by chance or due to the internal dynamics of the network. To evaluate the role of random temporal overlap, the spike trains were shuffled, and the percentages of spikes occurring within consecutive 100 ms windows of the shuffled spike trains were subtracted from the percentages of the origi-

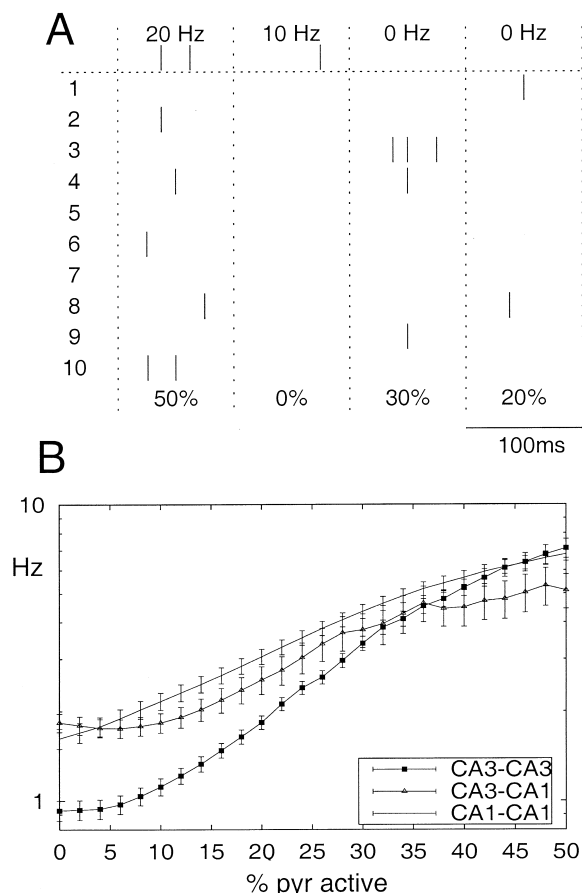


Figure 5. Nonlinear Relationship between Network Synchrony and Mean Firing Rate

(A) Illustration of rate and synchrony measurements in 11 neurons. Instant firing rates of a neuron (uppermost trace) in 100 ms windows are shown. Mean firing rates were estimated by averaging instant firing rates over many events at different levels of population synchrony. Population synchrony was determined as the percentage of the discharging cells (1–10). Note that this method determines rate and synchrony in the same time window but in nonoverlapping neurons.

(B) Mean firing rate (\pm SE) of neurons is displayed as function of population synchrony within the same region (CA3-CA3, $n = 336$, 18 sessions; CA1-CA1, $n = 189$, 11 sessions) and between CA3 and CA1 ($n = 143$, 19 sessions) regions, determined in time-shifted windows (100 ms) with 10 ms steps. Only recordings with at least ten pyramidal cells from the same region were used for synchrony measurement ($n = 5$ rats). Note that the relationship between population synchrony and firing rate is much steeper in the CA3 than in the CA1 region. Note also that the mean firing rate of CA1 neurons does not change until population synchrony of CA3 neurons exceeds 10% (trace CA3-CA1). Using either 50 or 200 ms windows, the results were similar (data not shown).

nal spike trains (Figure 6). This analysis revealed that the observed neuronal synchrony during CA1 ripples was larger than expected from random combination of spike coincidences. This was true for both the CA3 and CA1 regions. Furthermore, periods of very low synchrony also occurred more frequently than would be predicted by random discharges of neurons with identical spike dynamics as the original spike trains. These low-synchrony periods corresponded to no-ripple ep-

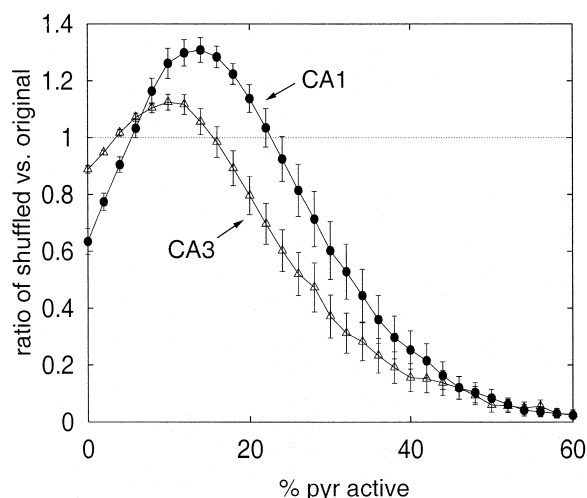


Figure 6. Population Synchrony Exceeds Values Expected from Random Coincidence of Uncorrelated Spike Trains

Synchrony was measured as the number of spiking neurons in 100 ms consecutive windows, and normalized density functions were calculated for both the original and time-shuffled spike trains. Shuffled data sets were generated by shifting spike trains by multiples of 100 ms periods (first spike train, 0 ms; second, 100 ms; third, 200 ms; etc.). The ratio of the two histograms was calculated and averaged for different recordings. Only recordings with at least ten pyramidal cells in the same region were included in these calculations (CA1, $n = 13$; CA3, $n = 23$).

ochs. Overall, both the synchrony firing rate relationship and the higher-than-chance incidence of high-synchrony states indicate that pyramidal cells display cooperative behavior, with higher cooperativity in the CA3 than the CA1 region.

Prediction of SPW Ripples from Ensemble Activity

The magnitude of the field oscillation event (peak of the rms of the event relative to baseline; see Experimental Procedures) was correlated with the spiking activity of CA1 and CA3 pyramidal cells. A multilinear regression method was used to quantify the relationship between the number of action potentials of the recorded cell population and the magnitude of ripple power. The number of action potentials was measured in a 100 ms time window centered at the peak of the ripple. Randomly selected subsets of the recorded cells in all possible combinations were used to calculate the mean (\pm SD) correlation coefficient for a given set of pyramidal cells. Correlation coefficients were calculated, and the relationship between spiking activity and the magnitude of the ripple event was examined as a function of the number of cells used for the calculation. Figure 7 illustrates recordings from 31 CA1 and 30 CA3 pyramidal cells. As expected, the accuracy of ripple prediction increased monotonically as a function of the number of neurons. In the CA3 region, the square of the regression coefficient showed a linear relationship with cell number (inset). In the CA1 region, a linear relationship was demonstrated between cell number and the third power of the correlation coefficients. Assuming that the observed correlations hold similarly for larger number of cells, recordings

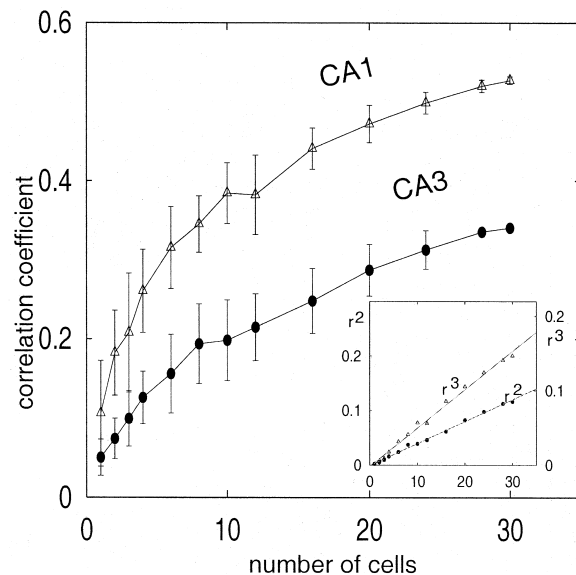


Figure 7. Reliability of Ripple Prediction Increases with the Size of Neuronal Populations

Multiple regression was used to calculate the relationship between ripple power in CA1 and the population synchrony for increasing number of neurons. For these calculations, a cross-validation procedure was used, in which the regression equation was calculated for the first half of the recording session and the correlation coefficient was calculated for the second half. Twenty-five randomly selected subsets of cells were used to calculate the correlation coefficient for a given cell ensemble. In this experiment, 30 CA3 and 31 CA1 pyramidal cells were recorded simultaneously. (Inset) Squared (CA3) or the third-power (CA1) values of the mean regression coefficient show a linear relationship with the number of cells.

from ~260 CA3 or 250 CA1 pyramidal cells would be required to accurately predict ($r > 0.9$) CA1 field ripples.

Discussion

The major conclusion from the present experiments is that a nonlinear interaction among the CA3 pyramidal neurons gives rise to an organized population burst, which in turn induces fast network oscillations in the CA1 population. Population bursts emerge first in/near the CA3a-b subregions and spread to the CA3c and CA1 regions. The degree of spatial synchrony of ripple events correlated with the magnitude of population spiking. At least 10% of the recorded CA3 neurons should discharge synchronously within a 100 ms window to exert a detectable influence on CA1 pyramidal cells at the population level.

Population Synchrony of CA3 Pyramidal Cells Triggers CA1 Ripples

We have defined synchrony as the percentage of the discharging neurons in a given time window. CA1 ripple-related synchrony correlated with the firing rate of both CA1 and CA3 pyramidal cells. Although the precise mechanisms of field ripple generation and associated discharge of CA1 pyramidal cells and interneurons is not known (Buzsaki et al., 1992; Ylinen et al., 1995; Traub and Bibbig, 2000), it is assumed that this CA1 event is

triggered by an enhanced activity of the CA3 inputs. A possible explanation for the enhanced drive of CA1 neurons is a random temporal coincidence of the discharging CA3 pyramidal cells. Another explanation is an organized population discharge within the CA3 network. Our findings support the latter scenario. Shuffling of the CA3 spike trains revealed that synchrony of the neuronal population exceeded values that might be expected from a random combination of spikes. Furthermore, while smaller amplitude field oscillations were different at the various recording sites, this difference diminished as the magnitude of field oscillations increased. Finally, the synchrony versus firing rate measurements also suggested nonrandom recruitment of neurons during synchronous states. It should be emphasized that, in these measurements, the neurons whose firing rates were being calculated were not included for the estimation of population synchrony to obtain an independent measurement of synchrony and firing rate.

In computer models, enhanced population bursts arise due to a progressively stronger recruitment of neurons in recurrent networks (Traub and Wong, 1982; Tsoodyks et al., 2000). In these models, population synchrony increases above what could be expected from firing rate changes alone. The nonlinear relationship between the ensemble discharge of neurons (i.e., synchrony) and their mean firing rates observed here supports the hypothesis that the recurrent excitatory connections of the CA3 pyramidal cells play a major role in the generation of SPW-related neuronal synchrony.

Spread of Activity in the CA3-CA1 Regions Reflects Functional Organization

The anatomical and functional organization of the intra-hippocampal system is often contrasted with the strict topographic connections of neocortical columns (Amaral and Witter, 1989). Indeed, very few physiological recordings from CA1 neurons indicate intraregional variation of discharge patterns (Eichenbaum et al., 1989; Hampson et al., 1996, 1999). In our experiments, the spread of excitatory activity from the CA3 to CA1 pyramidal cells could be monitored at the single neuron level. Activity of a portion of single CA3 pyramidal neurons differentially predicted the occurrence of ripple-related burst discharges of circumscribed groups of CA1 pyramidal cells.

The subtle but reliable location-dependent field unit correlations may be explained by various mechanisms. First, a nonhomogeneous distribution of Schaffer collateral terminals may differentially affect various parts of their CA1 target. Reconstruction of the axonal arbors of single CA3 pyramidal cells in vivo revealed CA1 sites with high bouton density alternating with areas with a low number of boutons (Li et al., 1994). At high-density locations, some target CA1 pyramidal neurons may be contacted by several synaptic release sites (Shepherd and Harris, 1998). Against these observations, one may hypothesize that synaptic connections between single CA3 pyramidal neurons and small groups of CA1 neurons were strong enough to exert a spatially differential effect within the CA1 neuronal population. Other data, on the other hand, argue against such a single-cell effect. First, only a small fraction of CA3 pyramidal cells

displayed location-dependent field correlations. When several neurons were recorded by the same tetrode, only one or none of the pyramidal neurons showed a differential correlation with CA1 sites. Second, synaptic connections between CA3-CA1 pyramidal cells are believed to be weak and unreliable (Sayer et al., 1989, 1990; Friedlander et al., 1990; Andersen et al., 1994). Finally, at the population level, >10% CA3 pyramidal cells had to discharge synchronously within 100 ms, which is the approximate duration of SPW-related synchrony, to exert an impact on the discharge frequency of CA1 pyramidal cells.

The second explanation is based on the hypothesis that SPW participation of CA3 pyramidal neurons is not random (Ylinen et al., 1995). According to this hypothesis, a given CA3 neuron preferentially and consistently discharges together with a selective group of other CA3 cells whose axons, in turn, converge differentially at the recorded CA1 sites. We assume that our CA3 pyramidal neurons with location-dependent CA1 field correlations represented such small groups. According to this hypothesis, the discharge of the recorded CA3 cell consistently correlated with the activity of other nonrecorded neurons and the axon terminals of this CA3 subgroup converged onto a circumscribed group of CA1 pyramidal cells. A logical extension of this hypothesis is that spike discharge of a given CA1 neuron during immobility and slow-wave sleep is typically brought about by the coherent discharge of the same small group of CA3 pyramidal cells. This functional interpretation gains support from previous observations that, during SPW ripples, selective subgroups of pyramidal cells discharge together in a short sequence (Wilson and McNaughton, 1994; Kudrimoti et al., 1999; Nadasdy et al., 1999). In summary, we suggest that the spatiotemporal discharge pattern of CA3 pyramidal cells is the cause for the spatial variability of ripple-related activity in the CA1 region. A prediction of this hypothesis is that the location-dependent relationship between CA3 and CA1 pyramidal neurons may be modified by behavioral training.

The third explanation for the observed single-cell field differences is that subsets of CA1 interneurons were differentially innervated by a single CA3 pyramidal cell, which, in turn, biased the field patterns. Indeed, we found high reliability of monosynaptic spike transmission between CA3 pyramidal cells and some CA1 interneurons (our unpublished data). However, interneurons showed equally high correlations with fields recorded from local and distal sites, indicating their more global involvement in population events. Therefore, interneuron mediation of the observed location-specific effect is less likely.

A macroscopic reflection of the anatomical organization was demonstrated by the differential involvement of neurons in the subregions of the CA3 field. During the SPW ripple event, neurons in the CA3a and b subregions discharged first, followed by CA3c and CA1 pyramidal cells. The magnitude of the CA1 ripple-related firing rate increase also followed the CA3a-b-c-CA1 sequence. These findings suggest that SPW bursts emerged in the CA3a-b subregions. Increased activity of these neurons recruited progressively more neurons in CA3c. Importantly, a similar recruitment gradient was also observed in the hippocampal slice preparation. After pharmaco-

logical blockage of GABA_A receptors, interictal spikes were initiated in CA2/CA3a and spread to CA3c (Wong and Traub, 1983). This network dynamics may be explained by the anatomical organization of the CA3 region. Although all subregions are interconnected by the recurrent collateral systems, the number of recurrent collaterals of CA3a and b neurons is several-fold larger than that of single CA3c neurons (Li et al., 1994). This may explain the mainly unilateral traffic from CA3a-b to CA3c neurons during SPW. Thus, a reasonable interpretation of our data is that the CA3a-b region acted as a "pacemaker" from which activity spread to both CA3c and CA1 neurons. In turn, the relatively large percentage of synchronously discharging CA3c pyramidal cells contributed to further depolarization of CA1 pyramidal cells. The 6 ms latency between population activity in CA3c and CA1 faithfully reflected the evoked spike transmission delay between these neurons (Winson and Abzug, 1977). The consistent relationship between field ripples in the CA1 pyramidal cell layer and sharp negative waves in the stratum radiatum (Ylinen et al., 1995) emphasizes the importance of the CA3c afferents. More than two-thirds of the axon collaterals of CA3c pyramidal cells project to the CA1 stratum radiatum (Li et al., 1994), whose cooperative activity brings about the field SPW. Thus, multiple recurrent loops within the CA3 region contribute to the population event underlying SPW.

Experimental Procedures

Surgery and Recording

The surgical procedures, electrode preparation, implantation, and spike sorting methods have been described (Csicsvari et al., 1998). In short, six male rats of the Sprague-Dawley strain (400–900 g) were implanted with either wire tetrodes (four animals) or silicon electrode arrays (two rats). They were anesthetized with a mixture (4 ml/kg) of ketamine (25 mg/ml), xylazine (1.3 mg/ml), and acepromazine (0.25 mg/ml) and placed in the stereotaxic apparatus. Electrodes were attached to a multidrive array and were implanted in the mediolateral direction, centered at AP = 3.5, ML = 2.5. In animals with wire tetrodes, eight independently movable, linearly arranged tetrodes were used with 300 μ m spacing in between them. In animals with silicon probes, the six-shank probe (300 μ m shank separation; four recording sites per shank, with 25 μ m vertical spacings) was implanted in the CA3 region, while CA1 neurons were monitored by two additional tetrodes. For both wire tetrodes and silicon probes, the most anterior CA1 electrode was 0.5–0.8 mm posterior to the last CA3 electrode, to maximize the probability that the terminal fields of the recorded CA3 neurons innervated the CA1 recording area (Li et al., 1994). Two 50 μ m single tungsten wires (with 2 mm of the insulation removed) were inserted into the cerebellum and served as ground and reference electrodes. After recovery from surgery, the electrodes were advanced to the CA1 and CA3 regions of the hippocampus within a week. Unit and field activities were recorded while the animal was immobile and sleeping in the home cage. Instrumentation amplifier dyes built in the female connector (32 channel, BAK Electronics, Inc., Germantown, MD) were used to reduce cable movement artifacts. A 64 channel DataMAX system (16 bit resolution; RC Electronics, Santa Barbara, CA) was used to continuously record electrical activity at 20 kHz. The recorded data (typically 4–12 giga bytes per session) were stored on DAT (DDS-3) tapes and analyzed offline using PC-linux computers and an IBM SP2 14 node parallel computer.

Spike Sorting

The continuously recorded wide-band signals were high-pass filtered (0.8–5 kHz) digitally. The power (root-mean-square) of the filtered signal was computed in a sliding window (0.2 ms) for spike detection. Spikes with power of more than five times the SD from

the baseline mean were extracted. The extracted spike waveforms were separated on the basis of their spike amplitude and wave-shape. The spike waveforms were reconstructed to 40 kHz by using the principles of the sampling theorem, and the peaks of the original and reconstructed waveforms were realigned. Principal component analysis (PCA) was used to extract features from the waveshapes. The first three principal components were calculated for each channel recorded by the electrode. Units were identified and isolated by a graphical clustering method referred to as "cluster cutting" (Wilson and McNaughton, 1994; Skaggs et al., 1996). Auto- and cross-correlations were calculated to verify the clustering procedure.

Detection of SPW-Associated Fast Ripples

The procedures described here were identical to those described earlier (Csicsvari et al., 1999b). The wide-band (1–5 kHz) recorded data was digitally band-pass filtered (80–250 Hz), and the power (root-mean-square) of the filtered signal was calculated for each electrode. The mean and standard deviation (SD) of the power signal were calculated to determine the detection threshold. Oscillatory epochs with a power of one or more SD above the mean were detected. The beginning and the end of oscillatory epochs were marked at points where the power fell below 0.5 SD. Theta periods, detected by using the theta-delta power ratio (Csicsvari et al., 1999a), were excluded from the analysis.

Population Synchrony and Discharge Rates

Synchrony was determined by measuring the number of discharging neurons in a given time window (5–100 ms contiguous epochs), independent of the number of spikes emitted by a given cell in the particular time window. Although fixed time windows can generate aliasing (binning) errors, in long recording sessions, similar time relations between spikes occur repeatedly and independently of the arbitrary windows. For examining the impact of synchrony on firing rate of neurons, both fixed and time-shifted windows were used (50 ms, 100 ms, and 200 ms windows; 10 ms steps). For these measurements, only recordings with at least ten pyramidal cells were used, and the recording sessions were 30–120 min (i.e., >18,000 windows). Firing rates of individual cells were determined in the same time window (Figure 5A). Determination of firing rates in short time segments required averaging from multiple events. For example, if a neuron discharged two spikes in ten successive 100 ms events, its rate was 2 Hz. When examining the relationship between population synchrony and firing rate, the neuron whose firing was estimated was excluded from the population synchrony measurement (i.e., for n cells, synchrony was measured for n combinations, each time for group of $n-1$ cells). This procedure was followed to obtain an independent measurement of synchrony and firing rate.

Histological Procedures

Following completion of the experiments, the rats were deeply anesthetized and perfused through the heart first with 9% saline solution followed by a 10% buffered formalin phosphate solution. The brains were sectioned by a vibratome at 100 μ m in the coronal plane. The sections were mounted on slides, Nissl stained, and coverslipped.

Acknowledgments

We thank K. Harris, D. Henze, and L. Marshall for their constructive comments on the manuscript. This work was supported by the National Institutes of Health (NS34994, MH54671, 1P41RR09754) and the Hara Foundation, Japan (H. H.). We thank J. Hetke and K. Wise for supplying us with silicon probes.

Received June 19, 2000; revised September 22, 2000.

References

Ahissar, E., Vaadia, E., Ahissar, M., Bergman, H., Arieli, A., and Abeles, M. (1992). Dependence of cortical plasticity on correlated activity of single neurons and on behavioral context. *Science* 257, 1412–1415.

Amaral, D.G., and Witter, M.P. (1989). The three-dimensional organi-

zation of the hippocampal formation, a review of anatomical data. *Neuroscience* 31, 571–591.

Andersen, P., Trommald, M., and Jensen, V. (1994). Low synaptic convergence of CA3 collaterals on CA1 pyramidal cells suggests few release sites. *Adv. Second Messenger Phosphoprotein Res.* 29, 340–351.

Bragin, A., Jando, G., Nadasdy, Z., van Landeghem, M., and Buzsaki, G. (1995). Dentate EEG spikes and associated interneuronal population bursts in the hippocampal hilar region of the rat. *J. Neurophysiol.* 73, 1691–1705.

Bullock, T.H., McClune, M.C., Achimowicz, J.Z., Iragui-Madoz, V.J., Duckrow, R.B., and Spencer, S.S. (1995). Temporal fluctuations in coherence of brain waves. *Proc. Natl. Acad. Sci. USA* 92, 11568–11572.

Buzsaki, G. (1989). Two-stage model of memory trace formation: a role for "noisy" brain states. *Neuroscience* 31, 551–570.

Buzsaki, G., and Chrobak, J.J. (1995). Temporal structure in spatially organized neuronal ensembles: a role for interneuronal networks. *Curr. Opin. Neurobiol.* 5, 504–510.

Buzsaki, G., Leung, L.W., and Vanderwolf, C.H. (1983). Cellular bases of hippocampal EEG in the behaving rat. *Brain Res.* 287, 139–171.

Buzsaki, G., Horvath, Z., Urioste, R., Hetke, J., and Wise, K. (1992). High-frequency network oscillation in the hippocampus. *Science* 256, 1025–1027.

Chrobak, J.J., and Buzsaki, G. (1994). Selective activation of deep layer (V–VI) retrohippocampal cortical neurons during hippocampal sharp waves in the behaving rat. *J. Neurosci.* 14, 6160–6170.

Chrobak, J.J., and Buzsaki, G. (1996). High-frequency oscillations in the output networks of the hippocampal-entorhinal axis of the freely behaving rat. *J. Neurosci.* 16, 3056–3066.

Csicsvari, J., Hirase, H., Czurko, A., and Buzsaki, G. (1998). Reliability and state-dependence of pyramidal cell-interneuron synapses in the hippocampus: an ensemble approach in the behaving rat. *Neuron* 21, 179–189.

Csicsvari, J., Hirase, H., Czurko, A., Mamiya, A., and Buzsaki, G. (1999a). Oscillatory coupling of hippocampal pyramidal cells and interneurons in the behaving rat. *Journal of Neuroscience* 19, 274–287.

Csicsvari, J., Hirase, H., Czurko, A., Mamiya, A., and Buzsaki, G. (1999b). Fast network oscillations in the hippocampal CA1 region of the behaving rat. *J. Neurosci.* 19, 1–4.

Deadwyler, S.A., Bunn, T., and Hampson, R.E. (1996). Hippocampal ensemble activity during spatial delayed-nonmatch-to-sample performance in rats. *J. Neurosci.* 16, 354–372.

Eichenbaum, H., Wiener, S.I., Shapiro, M.L., and Cohen, N.J. (1989). The organization of spatial coding in the hippocampus: a study of neural ensemble activity. *J. Neurosci.* 9, 2764–2775.

Friedlander, M.J., Sayer, R.J., and Redman, S.J. (1990). Evaluation of long-term potentiation of small compound and unitary EPSPs at the hippocampal CA3-CA1 synapse. *J. Neurosci.* 10, 814–825.

Hampson, R.E., Byrd, D.R., Konstantopoulos, J.K., Bunn, T., and Deadwyler, S.A. (1996). Hippocampal place fields, relationship between degree of field overlap and cross-correlations within ensembles of hippocampal neurons. *Hippocampus* 6, 281–293.

Hampson, R.E., Simeral, J.D., and Deadwyler, S.A. (1999). Distribution of spatial and nonspatial information in dorsal hippocampus. *Nature* 402, 610–614.

Hasselmo, M.E., Schnell, E., and Barkai, E. (1995). Dynamics of learning and recall at excitatory recurrent synapses and cholinergic modulation in rat hippocampal region CA3. *J. Neurosci.* 15, 5249–5262.

Ishizuka, N., Weber, J., and Amaral, D.G. (1990). Organization of intrahippocampal projections originating from CA3 pyramidal cells in the rat. *Comp. Neurol.* 295, 580–623.

Kudrimoti, H.S., Barnes, C.A., and McNaughton, B.L. (1999). Reactivation of hippocampal cell assemblies: effects of behavioral state, experience, and EEG dynamics. *J. Neurosci.* 19, 4090–4101.

Laurent, G. (1999). A systems perspective on early olfactory coding. *Science* 286, 723–728.

- Li, X.G., Somogyi, P., Ylinen, A., and Buzsaki, G. (1994). The hippocampal CA3 network: an in vivo intracellular labeling study. *J. Comp. Neurol.* 339, 181–208.
- Lisman, J.E. (1999). Relating hippocampal circuitry to function: recall of memory sequences by reciprocal dentate-CA3 interactions. *Neuron* 22, 233–242.
- Marr, D. (1971). Simple memory: a theory for archicortex. *Philos. Trans. R. Soc. Lond. B Biol. Sci.* 262, 23–81.
- McNaughton, N., and Morris, R.G. (1987). Chlordiazepoxide, an anxiolytic benzodiazepine, impairs place navigation in rats. *Behav. Brain Res.* 24, 39–46.
- McNaughton, B.L., Barnes, C.A., and O'Keefe, J. (1983). The contributions of position, direction, and velocity to single unit activity in the hippocampus of freely-moving rats. *Exp. Brain Res.* 52, 41–49.
- Muller, R.U., Kubie, J.L., and Ranck, J.B., Jr. (1987). Spatial firing patterns of hippocampal complex-spike cells in a fixed environment. *J. Neurosci.* 7, 1935–1950.
- Muller, R.U., Stead, M., and Pach, J. (1996). The hippocampus as a cognitive graph. *J. Gen. Physiol.* 107, 663–694.
- Nadasdy, Z., Hirase, H., Czurko, A., Csicsvari, J., and Buzsaki, G. (1999). Replay and time compression of recurring spike sequences in the hippocampus. *J. Neurosci.* 9, 9497–9507.
- O'Keefe, J., and Recce, M.L. (1993). Phase relationship between hippocampal place units and the EEG theta rhythm. *Hippocampus* 3, 317–330.
- Rolls, E.T. (1999). Spatial view cells and the representation of place in the primate hippocampus. *Hippocampus* 9, 467–480.
- Sayer, R.J., Redman, S.J., and Andersen, P. (1989). Amplitude fluctuations in small EPSPs recorded from CA1 pyramidal cells in the guinea pig hippocampal slice. *J. Neurosci.* 9, 840–850.
- Sayer, R.J., Friedlander, M.J., and Redman, S.J. (1990). The time course and amplitude of EPSPs evoked at synapses between pairs of CA3/CA1 neurons in the hippocampal slice. *J. Neurosci.* 10, 826–836.
- Shepherd, G.M., and Harris, K.M. (1998). Three-dimensional structure and composition of CA3→CA1 axons in rat hippocampal slices: implications for presynaptic connectivity and compartmentalization. *J. Neurosci.* 18, 8300–8310.
- Skaggs, W.E., McNaughton, B.L., Wilson, M.A., and Barnes, C.A. (1996). Theta phase precession in hippocampal neuronal populations and the compression of temporal sequences. *Hippocampus* 6, 149–172.
- Tanila, H., Shapiro, M.L., and Eichenbaum, H. (1997). Discordance of spatial representation in ensembles of hippocampal place cells. *Hippocampus* 7, 613–623.
- Traub, R.D., and Bibbig, A. (2000). A model of high-frequency ripples in the hippocampus based on synaptic coupling plus axon-axon gap junctions between pyramidal neurons. *J. Neurosci.* 20, 2086–2093.
- Traub, R.D., and Wong, R.K. (1982). Cellular mechanism of neuronal synchronization in epilepsy. *Science* 216, 745–747.
- Tsodyks, M.V., Uziel, A., and Markram, H. (2000). Synchrony generation in recurrent networks with frequency-dependent synapses. *J. Neurosci.* 20, RC50.
- Wiebe, S.P., and Staubli, U.V. (1999). Dynamic filtering of recognition memory codes in the hippocampus. *J. Neurosci.* 19, 10562–10574.
- Wilson, M.A., and McNaughton, B.L. (1994). Reactivation of hippocampal ensemble memories during sleep. *Science* 265, 676–679.
- Winson, J., and Abzug, C. (1977). Gating of neuronal transmission in the hippocampus: efficacy of transmission varies with behavioral state. *Science* 6, 1223–1225.
- Wong, R.K., and Traub, R.D. (1983). Synchronized burst discharge in disinhibited hippocampal slice. I. Initiation in CA2-CA3 region. *J. Neurophysiol.* 49, 442–458.
- Ylinen, A., Bragin, A., Nadasdy, Z., Jando, G., Szabo, I., Sik, A., and Buzsaki, G. (1995). Sharp wave-associated high-frequency oscillation (200 Hz) in the intact hippocampus: network and intracellular mechanisms. *J. Neurosci.* 15, 30–46.